Probing the electrical properties of highly-doped Al:ZnO nanowire ensembles

Rodrigo Noriega,[1] Jonathan Rivnay,[2] Ludwig Goris,[2] Daniel Kälblein,[3] Hagen Klauk,[3] Klaus Kern,[3,4] Linda M. Thompson,[5] Aaron C. Palke,[5] Jonathan F. Stebbins,[5] Jacob R. Jokisaari,[6] Greg Kusinski,[6] and Alberto Salleo[2,a)]

[1]*Department of Applied Physics, Stanford University, Stanford, California 94305, USA*
[2]*Department of Materials Science and Engineering, Stanford University, Stanford, California 94305, USA*
[3]*Max Planck Institute for Solid State Research, Heisenbergstrasse 1, 70569 Stuttgart, Germany*
[4]*Institut de Physique des Nanostructures, Ecole Polytechnique Fédérale de Lausanne, 1015 Lausanne, Switzerland*
[5]*Department of Geological and Environmental Sciences, Stanford University, Stanford, California 94305, USA*
[6]*School of Materials Science and Engineering, Clemson University, Clemson, South Carolina 29634, USA*

(Received 27 September 2009; accepted 22 January 2010; published online 15 April 2010)

The analysis of transparent conducting oxide nanostructures suffers from a lack of high throughput yet quantitatively sensitive set of analytical techniques that can properly assess their electrical properties and serve both as characterization and diagnosis tools. This is addressed by applying a comprehensive set of characterization techniques to study the electrical properties of solution-grown Al-doped ZnO nanowires as a function of composition from 0 to 4 at. % Al:Zn. Carrier mobility and charge density extracted from sensitive optical absorption measurements are in agreement with those extracted from single-wire field-effect transistor devices. The mobility in undoped nanowires is 28 $cm^2/V\,s$ and decreases to ~ 14 $cm^2/V\,s$ at the highest doping density, though the carrier density remains approximately constant (10^{20} cm^{-3}) due to limited dopant activation or the creation of charge-compensating defects. Additionally, the local geometry of the Al dopant is studied by nuclear magnetic resonance, showing the occupation of a variety of dopant sites. © *2010 American Institute of Physics*. [doi:10.1063/1.3360930]

I. INTRODUCTION

Transparent conducting oxides (TCO) have been the focus of intense research in recent years,[1] due to their applications in electronics and photovoltaics. These wide-bandgap materials have been used as the active channel material for field-effect transistors,[2,3] as the electron-accepting material in dye-sensitized solar cells,[4] and, when doped, as transparent electrodes for transistors, organic light emitting diodes, solar cells, and electrochromic windows.[5] The most widely used TCO is indium-tin oxide (ITO). However, due to high processing costs and indium scarcity there has been a field-wide push to find a suitable alternative. Zinc oxide (ZnO) is an extensively studied material[6] and well-suited to replace ITO, due to its low cost and marginal toxicity combined with its competitive electrical and optical properties. Without any intentional doping, ZnO is naturally n-type and can be extrinsically doped by introducing heteroatoms (such as Al, Ga, In, B, or Sn) into the ZnO crystal lattice, reaching carrier concentrations as high as 1.5×10^{21} cm^{-3}.[6] Electron mobility in ZnO can reach values of 200 $cm^2\,V^{-1}\,s^{-1}$ for ZnO single crystals at low doping levels, with mobility generally decreasing at higher doping levels. However, for heavily doped ZnO films obtained with techniques such as magnetron sputtering, pulsed laser deposition, and metal-organic chemical vapor deposition, the mobility varies between 10 $cm^2\,V^{-1}\,s^{-1}$ and 60 $cm^2\,V^{-1}\,s^{-1}$ depending on the microstructure of the material.[6] The lowest resistivity achieved in ZnO is on the order of 10^{-4} Ω cm, comparable to ITO.[6]

Recent research has focused on tailoring the properties of these materials by modifying their morphology at the nanoscale.[4,7] ZnO has a wurtzite crystal structure comprised of a series of alternating planes of tetrahedrally coordinated O^{2-} and Zn^{2+} ions stacked along the c-axis, with characteristic polar surfaces that give rise to a number of different nanostructures including rods, wires, belts, springs, and tubes.[7]

The key qualities of TCOs are their optical transmission in the visible and near-IR and their electrical conductivity. Films made of networks of doped ZnO nanowires have been shown to have potential to be used as a TCO in photovoltaics; as long as the sheet resistance value can be decreased to compete with other transparent electrode materials, while maintaining a high transparency. Doped ZnO nanowire mats exhibit currently a sheet resistance of 10^3 Ω/□ combined with 80%–85% transmission.[8,9] For flexible substrates, the benchmark values of sheet resistance and light transmission for non-ITO materials have been set by carbon nanotube networks[10] (200 Ω/□ and 85%, respectively), and silver nanowire meshes[11] (10 Ω/□ and 80%). Conduction through networks of quasi-one-dimensional (1D) structures depends on charge transport through each element and on charge transfer from one element to the next; at this point we will focus on the conduction within individual doped ZnO nanowires.

a)Electronic mail: asalleo@stanford.edu.

In n-ZnO, the conductivity is approximated as $\sigma \approx e\mu_e N_e$, where e is the elementary charge; μ_e and N_e are the electron mobility and concentration, respectively. Accordingly, proper characterization of a TCO's conductivity requires quantitative determination of the density and mobility of the charge carriers. The carrier concentration and mobility in semiconducting thin films are typically obtained using Hall effect measurements, whose application is problematic for extracting electrical characteristics from quasi-1D structures such as nanowires. As an alternative, single-wire field effect transistors (SWFET) have been used to measure carrier mobility.[2,12–19] In this technique, only a single device (i.e., a single wire) can be measured at a time, making the collection of data from a set of nanowires a labor-intensive and time-consuming process. This technique is also hindered by additional issues associated with the deposition of electrical contacts on nanomaterials, including the effects of contact resistance and the alteration of the material's properties (such as unintentional doping and/or damage caused by the ion or electron beam) that must be taken into account during measurement interpretation.

The mobility (μ_e) and free carrier density (N_e) in aluminum-doped ZnO (AZO) films can also be measured using polarized light ellipsometry.[20,21] Ellipsometry experiments have the advantage of being a noncontact technique, therefore, avoiding the unintentional modification of the sample. However, values extracted from ellipsometry depend on the accurate measurement of the change in the polarization state of light reflected from the sample surface. Because nanowire films are rough and scatter light effectively, the validity of ellipsometry experiments is compromised.

Fourier-transform infrared spectroscopy (FTIR) (Refs. 22 and 23) or attenuated total reflection FTIR (Ref. 24) have also been used to analyze the free carrier absorption in ZnO films. For highly scattering films, however, the detected signal attenuation is not necessarily correlated with the absorption of the sample alone.

These issues pose a need for a better way to measure the electrical properties of an ensemble of nanowires, which we address by applying a comprehensive set of spectroscopic techniques to the characterization of highly Al-doped ZnO nanowires obtained with a solution-based low-temperature process.[8,25]

II. EXPERIMENTS

Previous studies of these nanowires using spatially-resolved analytical techniques such as Auger electron spectroscopy and energy-dispersive x-ray spectroscopy confirmed that the aluminum dopant is incorporated into the nanowires. High-resolution transmission electron microscopy was used to show that the as-synthesized nanowires are highly crystalline with the growth axis being the c-axis of the ZnO wurtzite crystal [Fig. 1(c)].[8,25] Typical dimensions for the nanowires are diameters in the 20–80 nm range, and lengths of up to a few microns [Fig. 1(d)].[8,25]

The Al:Zn ratio in the product material is determined using an inductively-coupled plasma atomic emission spectrometer (ICP-AES). Films of AZO nanowires were prepared on quartz substrates by drop-casting from an ethanol suspension. The electrical properties of nanowire ensembles were obtained by applying the Drude model[26] for metals to the absorption spectrum of these films measured using photothermal deflection spectroscopy (PDS) (Refs. 27 and 28) and subsequently compared to SWFET measurements. Finally, the coordination environment of dopant atoms was investigated using ^{27}Al solid-state nuclear magnetic resonance (NMR).

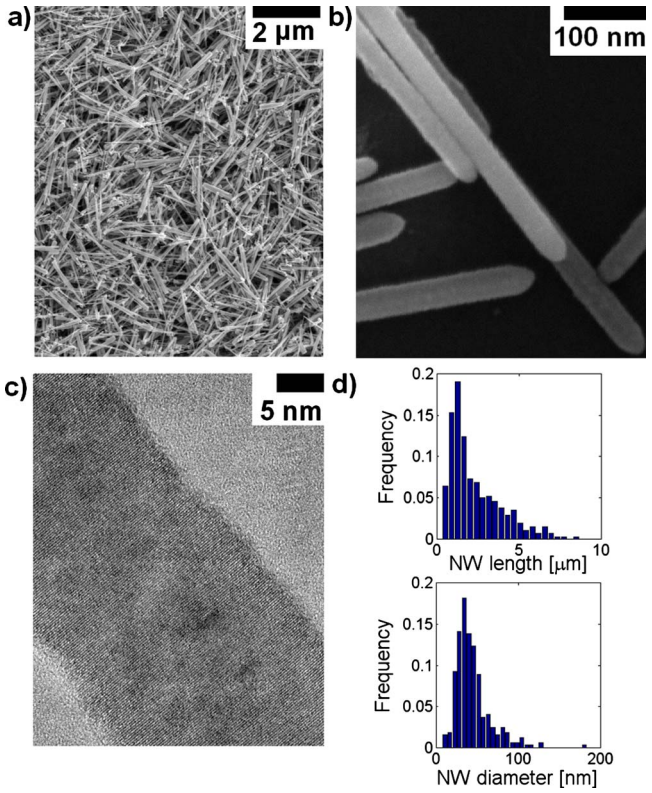

FIG. 1. (Color online) Scanning electron micrographs [(a), (b)] showing representative samples of the synthesized nanowires. High resolution electron microscopy (c) shows the crystallinity of the solution grown nanowires. The length and diameter statistics for a population of ~350 nanowires are also shown (d).

A. Synthesis process

0.104 M solutions of zinc acetate [$Zn(C_2H_3O_2)_2$, Sigma Aldrich] in trioctylamine ([$CH_3(CH_2)_7]_3N$, Sigma Aldrich) with varying amounts of basic aluminum diacetate [$Al(OH)(C_2H_3O_2)_2$, Sigma Aldrich] were prepared in a three-necked flask. The reaction mixture was kept under a continuous N_2 flow and refluxed at 300 °C for 3 h. The synthesis products were centrifuged at 6000 rpm. Subsequently, the supernatant was discarded and the precipitates were resuspended in ethanol, filtered over nylon membranes with porosities of 100 and 40 μm, and precipitated out by additional centrifugation steps. The final product was left to dry and placed into vials for subsequent characterization.[8,25]

Low-temperature solution-based synthesis processes are attractive due to their relative simplicity, low cost, and scalability but they also have significant drawbacks, particularly

a higher inhomogeneity in morphology and doping when compared to more strictly controlled processes (i.e., chemical vapor deposition).

B. ICP-AES

A small portion of each powdered sample was dissolved in a 2% HCl aqueous solution, and the detected intensities of the spectral lines were calibrated with standards of Al and Zn, also in a 2% HCl aqueous solution.

C. PDS

PDS relies on the complete or fractional conversion of absorbed electromagnetic radiation by the material of interest into heat via nonradiative de-excitation processes. This conversion process causes a temperature rise in the material itself and its surroundings. The temperature rise leads to a localized change in the index of refraction in the surrounding deflection medium, which is measured and correlated with the absorption coefficient of the material of interest. During a measurement, a modulated monochromatic pump beam (arranged perpendicular to the plane of the substrate) is absorbed by the sample. A second (transverse) probe laser beam is deflected by the localized change in the refractive index of the surrounding deflection medium, and a position sensitive detector records the periodic deflection by a lock-in technique. The measured deflection is proportional to the absorption coefficient of the measured thin film.

Films were deposited from ethanol-based solutions of the nanowire powders onto quartz substrates and immersed in a cuvette filled with Fluorinert™ (3M). The pump beam was obtained from either a halogen or xenon lamp (for different energy ranges), then monochromated and focused onto the sample. The probe beam is a commercial He:Ne laser, and the deflection signal is measured with a position sentitive detector.

D. Single-nanowire FETs

SWFETs were fabricated by dispersing AZO nanowires onto heavily doped, thermally oxidized silicon substrates (with the substrate serving as the gate and the 200 nm thick SiO_2 as the gate dielectric) and preparing source/drain contacts on the wires by electron-beam lithography, metal evaporation, and lift-off.

E. NMR

Spectra were obtained from powder samples using a 14.1 T magnet with magic angle spinning (MAS) to reduce peak broadening, with sample spinning rates of 20 kHz, rf tip angle (solids) of about 30° (0.2 μs pulse), pulse delay of 0.1 s, and referenced to a 0.1 M $Al(NO_3)_3$ standard. The $ZnAl_2O_4$ spinel sample was synthesized by heating reagent grade $Al(OH)_3$ and ZnO at 1400 °C in air for 24 h.[29] All measurements were performed at room temperature.

III. RESULTS AND DISCUSSIONS

To investigate the effect of dopant concentration, ZnO nanowires with varying aluminum content were synthesized from solutions containing dopant amounts of 1, 3, 5, and 7 at. %. The average incorporation rate (at. % in the nanowires versus at. % in the synthesis solution) is 60%, and the dopant content in the nanowires ranges from 0.7 to 4 at. %. This confirms that the materials are heavily doped and the dopant incorporation rate is very high, which is remarkable given the low synthesis temperature (300 °C). In addition, undoped nanowires were also synthesized without adding dopant atoms into the synthesis bath in order to confirm that the observed improvement in conductivity is caused by the inclusion of aluminum atoms in the ZnO.

The solubility limit of aluminum in the ZnO wurtzite lattice is still somewhat controversial,[30–32] with reported values on the order of 1 at. %, corresponding to a carrier concentration of 4.1×10^{20} cm^{-3} for singly-ionized impurities, or 25% of the maximum reported concentration in thin films. It should be noted that different synthesis techniques work at different points in the phase diagram, and the maximum attainable doping level therefore depends on the specific growth process. Moreover, the thermodynamic solubility limit can be exceeded in nonequilibrium situations. In addition, as reported by Minami *et al.*,[33] the high carrier concentrations in AZO films are not always due only to impurities but also to intrinsic donor states.

A. Drude metal model

Such large free-carrier concentrations make AZO behave like a Drude metal,[34] making it possible to determine crucial properties such as free charge concentration and mobility using optical spectroscopic techniques. The Drude model predicts that the free charge density of a metal determines a cut-off frequency, the plasma frequency ω_p, such that for $\omega > \omega_p$ the material is practically transparent, and for radiation with $\omega < \omega_p$ the absorption coefficient and the reflectivity of the material are very high. There are two key parameters in this model: the plasma frequency and carrier scattering time

$$\omega_p \equiv \sqrt{\frac{N_e e^2}{m_e^* \varepsilon_0}}, \quad \tau \equiv \frac{\mu_e m_e^*}{e}, \tag{1}$$

where m_e^* is the effective electron mass at the bottom of the conduction band, and ε_0 is the permittivity of vacuum. For ZnO with 1 at. % of active dopants and an electron effective mass of $m_e^*=0.27m_e$ (where m_e is the electron's rest mass),[35] the plasma frequency is close to $\upsilon_p=\omega_p/2\pi=3.5\times10^{14}$ Hz, corresponding to a wavelength of $\lambda_p=860$ nm. Further refinement of this model can account for variability within each sample, assuming that the population of measured wires follows a Gaussian distribution for the mobility and free electron concentration. In this case, the measured (effective) absorption spectra α_{eff} will be a weighed superposition as follows

$$\alpha_{\text{eff}}(\lambda) = \frac{1}{2\pi\sigma_\mu\sigma_{N_e}}\int_0^\infty \int_0^\infty e^{-1/2[(\upsilon-\mu_o)^2/\sigma_\mu^2+(\eta-N_o)^2/\sigma_{N_e}^2]}\alpha_{\text{Drude}}(\lambda,\upsilon,\eta)d\eta d\upsilon, \quad (2)$$

where μ_o (N_o) and σ_μ (σ_{N_e}) are the average value and standard deviation for the mobility (free charge density) distribution, and $\alpha_{\text{Drude}}(\lambda,\mu,N_e)$ is the Drude model free carrier absorption at a wavelength λ for a material with a mobility (free electron density) of μ (N_e); υ and η are dummy integration variables.

B. PDS

In order to overcome problems associated with many traditional methods for measuring electrical properties in ZnO nanowire thin films, we have used transverse PDS.[27,28] PDS has the advantages of being a noncontact and nondestructive technique that enables the measurement of the optical properties of an entire ensemble of nanowires in a single experiment. It should be noted that when the free charges absorb the incoming light from the PDS pump beam, their oscillation amplitude is well inside a single nanowire, so the properties we obtain from these measurements correspond to an average over an ensemble of single AZO nanowires.

The measured spectra can be divided into three distinct regions (Fig. 2). The first region corresponds to free carrier absorption ($\hbar\omega < 2$ eV). Here, the increase in absorption coefficient in the IR is due to free charge carriers present in the material. Region 2 illustrates defect-related absorption ($\hbar\omega \sim 2-3$ eV, see Fig. 2 inset). Samples are mostly transparent in the visible region but a pronounced absorption band ~2.5 eV (500 nm) can be observed, most likely due to the incorporation of Al into the lattice of ZnO (such a band is absent in the undoped ZnO nanowires). Further study is necessary to clarify the exact origin of the defect-related absorption phenomena in these materials and their dependence on dopant inclusion. Region 3 corresponds to the absorption edge ($\hbar\omega > 3$ eV).

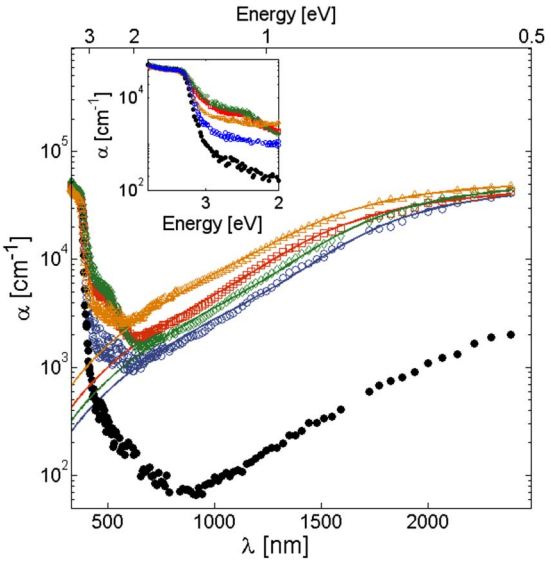

FIG. 2. (Color online) PDS spectra of ZnO nanowire films (● undoped, ○ 0.68 at. % Al, □ 1.58 at. % a Al, ◇ 2.34 at. % Al., △ 3.98 at. % Al) and the corresponding Drude model fits (solid lines). Inset: absorption coefficient vs photon energy in the band edge and sub-bandgap regions.

The low-energy region of each absorption spectrum was fitted using the Drude model as described above, with the fitting parameters being the average values and standard deviations μ_o, N_o, σ_μ, and σ_{N_e}. A similar approach was used to measure the interfacial charge in transparent, nonscattering ZnO field-effect transistors by Kim *et al.*[23] Since the amount of dopant in the nanowires is significant, a third approach considering the nonparabolicity of the conduction band[36,37] was used as well but showed no significant difference with the results presented here and was therefore not included. The mean values for the mobility (free charge density) distributions (Fig. 3) are in the range 27–14 $\text{cm}^2\,\text{V}^{-1}\,\text{s}^{-1}$ ($8.8-11.6\times10^{19}$ cm^{-3}), with standard deviations close to 2 $\text{cm}^2\,\text{V}^{-1}\,\text{s}^{-1}$ and 3×10^{19} cm^{-3}, with the exception of the 1.58 at. % Al:Zn sample (6.7 $\text{cm}^2\,\text{V}^{-1}\,\text{s}^{-1}$ and 5.5×10^{19} cm^{-3}) which can be explained by a larger degree of variability in the synthesis products compared to other (and better optimized) synthesis runs.

C. FET measurements

Because undoped ZnO does not display free carrier absorption, the value of the carrier mobility in undoped ZnO nanowires was measured using a SWFET device. The possible presence of unknown amounts of trapped charge at the nanowire/dielectric interface prevented us from estimating the residual free carrier density using SWFET measurements. Also, the calculation of the true gate capacitance is particularly important since it directly affects the calculated mobility value. However, the capacitance can be estimated by either using a finite-element model to calculate the gate capacitance or, alternatively, one can use the formula for a semiconducting cylinder embedded in a dielectric using an effective dielectric constant to account for the differences in geometry.[38] The gate capacitance per unit length in our devices was ~50 pF m^{-1}.

Nanowires used for the SWFET characterization were randomly chosen from a sample obeying the distribution showed in Fig. 1(d). They were well within the range of diameter and length earlier stated, as confirmed by SEM (see Fig. 4 inset). Analysis of the transfer curves (Fig. 4) indicates that the device has an on/off ratio of $\sim10^6$, with a mobility close to 28 $\text{cm}^2\,\text{V}^{-1}\,\text{s}^{-1}$, and an off-current on the order of 10^{-13} A. Comparing these results to similar devices previously reported,[13,14,16] which were synthesized by chemical vapor deposition methods at higher temperatures (700–950 °C), our on/off ratio is two to three orders of magnitude higher, with comparable mobilities. The low off-

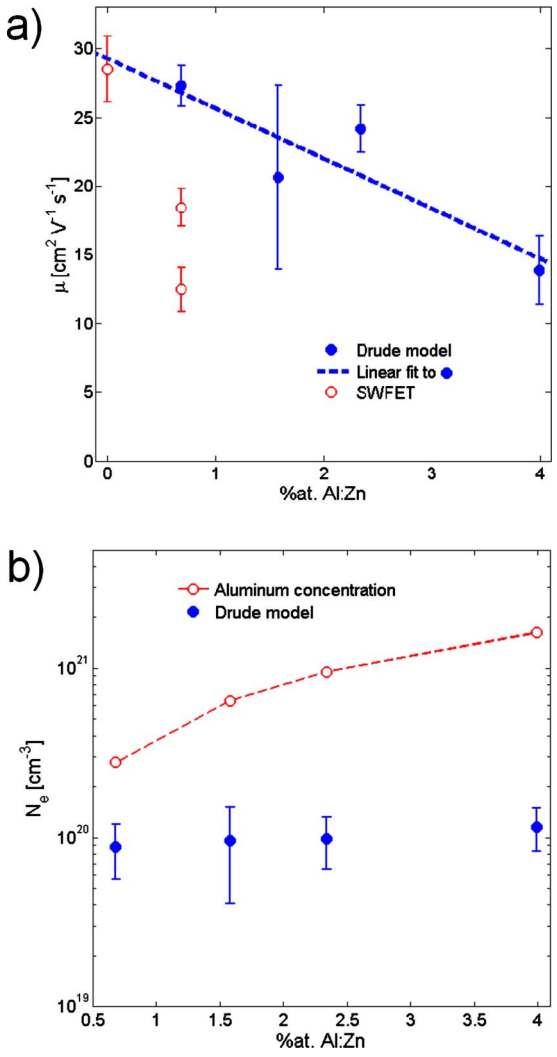

FIG. 3. (Color online) a) Carrier mobility calculated from SWFET measurements (○), as well as values obtained with the Drude model fits (●). (b) Concentration of aluminum atoms (○) for various doped ZnO nanowires compared to the free-carrier density calculated with the Drude model fits (●). Error bars are ± one standard deviation.

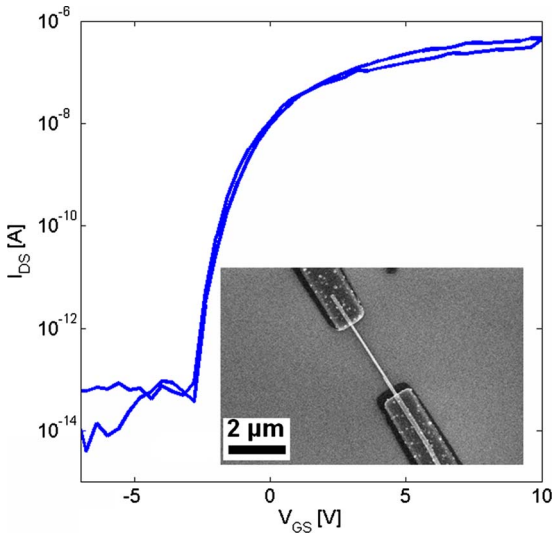

FIG. 4. (Color online) Transfer curve of an undoped ZnO nanowire FET with a drain-source voltage $V_{DS}=1$ V (inset: SEM image of the device). The SWFET devices are fabricated from typical AZO nanowires (Fig. 1).

current of our device suggests that the synthesized wires are highly crystalline and have a low density of defects as these would typically lead to residual conductivity. ZnO SWFETs with various device structures reported elsewhere[3,12–14,16–19] have on/off ratios in the range 10^3-10^8, with the higher end being for devices employing an ozone post-treatment with a self-assembled superlattice as the dielectric.[18] The dimensions of the channels are comparable in all devices. SWFET devices with doped nanowires were also fabricated to confirm that the inclusion of Al in the material leads to increased conductivity. The minimum resistivity of our material measured optically was 2.6×10^{-3} Ω cm for wires with 0.68 at. % Al, which agrees with previous reports.[6]

Due to the short length of our nanowires (1–5 μm), it is difficult to fabricate multicontact SWFET devices to account for contact resistance. This prevents us from accurately determining the nanowire resistivity and mobility (and thus, free charge concentration). When comparing the mobility values obtained from PDS to those of SWFETs, it should be noted that contact resistance in FET devices results in an underestimation of the field effect mobility.[39] Two different SWFET devices are shown to demonstrate their variability, and the discrepancy with the values fitted using the Drude model (by a factor of 1.4–2.2) is explained by the fact that they are not corrected for contact resistance effects. In general, extracting materials properties from device measurements introduces issues associated with spurious nonideal effects. Given these considerations, the values obtained with the available measurements can be considered in agreement with the values extracted from the optical data (Fig. 3), showing that the electron mobility in the AZO nanowires is lowered by the presence of dopant levels. Also, the observed carrier density in all the samples is lower than expected if all the aluminum present in the nanowires was in zinc substitutional sites (Al_{Zn}), which would add one electron to the conduction band per each aluminum atom.

D. NMR

The oxidation state of Al, hence its electrical activity, is determined by its position in the lattice. The carrier concentration data suggest that not all Al atoms occupy donor sites within the lattice, with the remaining (inactive) Al creating defects that do not contribute to the free electron density and instead hinder charge transport by acting as scattering centers. In order to study the local environment of the Al atoms, we used ^{27}Al NMR. Historically, the active sites are thought to be substitutional in tetrahedrally coordinated zinc sites but solid state ^{27}Al NMR data indicates a far richer solid state chemistry that warrants further investigation.

^{27}Al MAS NMR spectra of all samples are dominated by three partially overlapping components (Fig. 5). The peak at about 10 ppm corresponds to Al sites with six oxygen neighbors (^{VI}Al), and is mainly comprised of a narrower peak with the same position and width as that of $ZnAl_2O_4$ spinel,[29] suggesting that this phase may be present. The amount of this secondary phase, however, must be lower than the detection limit of other analytical techniques that were used to

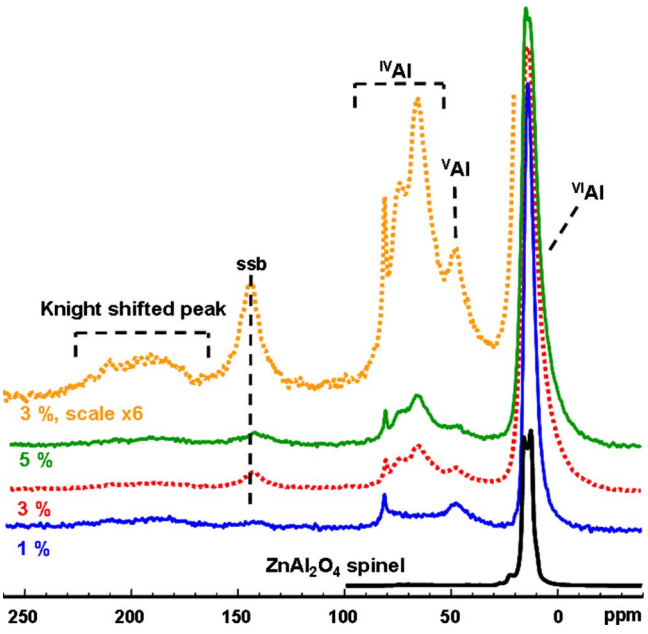

FIG. 5. (Color online) ^{27}Al MAS NMR spectra for Al-doped ZnO (at. % Al:Zn as labeled), collected at 14.1 T (156.5 MHz), with sample spinning rates of 20 kHz, rf tip angle (solids) of about 30° (0.2 μs pulse), pulse delay of 0.1 s, and referenced to 0.1 M $Al(NO_3)_3$. The only prominent spinning sideband (spin echo) in the range plotted, identified by varying the spinning rate, is marked by "ssb."

characterize the material.[8] Broad peaks from near 30 to 50 ppm, and 60 to 80 ppm, are most likely due to ^{V}Al and ^{IV}Al incorporated in the ZnO, with the latter having been reported in a previous NMR study.[31] A very narrow peak at 81.5 ppm suggests a small amount of Al in a highly symmetrical ^{IV}Al site. The observed ^{VI}Al peak overlaps that known for α-alumina but the formation of this phase is unlikely at the low temperatures of synthesis. The ^{IV}Al and ^{VI}Al peaks have different widths and positions from those typical of disordered crystalline phases such as γ-alumina,[40] indicating that these could make at most only a minor contribution to the spectra.

Spectra of all samples showed a low, broad peak centered around 180 ppm, contributing approximately 3%–7% of the total signal (from high to low Al dopant levels). This frequency is far outside the known range of normal chemical shifts in oxides, and must, therefore, be due to either the magnetic effects of unpaired electron spins, or, more likely, to a Knight shift from the conduction electrons. In fact, a previous low-resolution NMR study of Al-doped ZnO reported an ^{27}Al peak that was Knight shifted by about 200 ppm.[41] These results illustrate that aluminum as a dopant in our ZnO nanowires appears in various coordination environments; the determination of which ones are electrically active is beyond the scope of this study and will be the object of another publication.

IV. CONCLUSION

We have used a wide-ranging set of characterization techniques to study ensembles of TCO nanowires, which allowed us to show that ZnO nanowires can be effectively doped with aluminum at low temperature (300 °C) and the properties of the obtained materials have been measured. The electron mobility in the highly doped Al:ZnO nanowires decreases noticeably with increasing Al concentration, due to the Al acting as scattering centers. The free charge carrier density, however, shows no significant dependence on the Al:Zn ratio, which suggests either a limited activation of the dopant in the ZnO lattice or the appearance of compensating defects. NMR spectroscopy shows that aluminum can occupy a rich variety of sites and suggests that not all are electrically active. The measured properties (μ_e, ρ) of these solution-grown nanostructured materials are comparable[6] to ZnO single crystals grown by high-temperature vapor-phase or hydrothermal methods, doped either during synthesis or with ion diffusion into intrinsic ZnO crystals. Improved dopant activation without a further decrease in mobility in these AZO nanowires would result in conductivities rivaling those of ITO and AZO thin films ($\sim 10^{-4}$ Ω cm).

The results obtained point out the need to understand the dopant incorporation and activation mechanisms as well as the charge transport process in nanostructured ZnO, and establish a combination of techniques that allows the effective, reliable, and comprehensive characterization of an ensemble of nanowires.

ACKNOWLEDGMENTS

This research was supported by the King Abdullah University of Science and Technology (KAUST): Global Research Partnership (GRP) through the Center for Advanced Molecular Photovoltaics (CAMP), the Global Climate and Energy Project (GCEP) through Stanford University and the Department of Energy (Solar America Initiative). We thank Ted Trigg for his collaboration and Craig H. Peters for helpful discussions in preparing this manuscript.

[1] D. S. Ginley and C. Bright, MRS Bull. **25**, 15 (2000).
[2] S. Y. Ju, A. Facchetti, Y. Xuan, J. Liu, F. Ishikawa, P. D. Ye, C. W. Zhou, T. J. Marks, and D. B. Janes, Nat. Nanotechnol. **2**, 378 (2007).
[3] B. N. Pal, P. Trottman, J. Sun, and H. E. Katz, Adv. Funct. Mater. **18**, 1832 (2008).
[4] M. Law, L. E. Greene, J. C. Johnson, R. Saykally, and P. D. Yang, Nature Mater. **4**, 455 (2005).
[5] B. G. Lewis and D. C. Paine, MRS Bull. **25**, 22 (2000).
[6] K. Ellmer, J. Phys. D **34**, 3097 (2001).
[7] Z. L. Wang, J. Phys.: Condens. Matter **16**, R829 (2004).
[8] L. Goris, R. Noriega, M. Donovan, J. Jokisaari, G. Kusinski, and A. Salleo, J. Electron. Mater. **38**, 586 (2009).
[9] R. Noriega, L. Goris, J. Rivnay, J. Scholl, L. M. Thompson, A. C. Palke, J. F. Stebbins, and A. Salleo, Proc. SPIE **7411**, 7411–24 (2009).
[10] M. W. Rowell, M. A. Topinka, M. D. McGehee, H. J. Prall, G. Dennler, N. S. Sariciftci, L. B. Hu, and G. Gruner, Appl. Phys. Lett. **88**, 233506 (2006).
[11] J. Y. Lee, S. T. Connor, Y. Cui, and P. Peumans, Nano Lett. **8**, 689 (2008).
[12] S. N. Cha, J. E. Jang, Y. Choi, G. A. J. Amaratunga, G. W. Ho, M. E. Welland, D. G. Hasko, D. J. Kang, and J. M. Kim, Appl. Phys. Lett. **89**, 263102 (2006).
[13] P. C. Chang, C. J. Chien, D. Stichtenoth, C. Ronning, and J. G. Lu, Appl. Phys. Lett. **90**, 113101 (2007).
[14] P. C. Chang, Z. Fan, C. J. Chien, D. Stichtenoth, C. Ronning, and J. G. Lu, Appl. Phys. Lett. **89**, 133113 (2006).
[15] Y. Cui, X. F. Duan, J. T. Hu, and C. M. Lieber, J. Phys. Chem. B **104**, 4766 (2000).
[16] Z. Y. Fan, D. W. Wang, P. C. Chang, W. Y. Tseng, and J. G. Lu, Appl. Phys. Lett. **85**, 5923 (2004).
[17] S. Ju, K. Lee, M. H. Yoon, A. Facchetti, T. J. Marks, and D. B. Janes, Nanotechnology **18**, 1 (2007).

[18]S. H. Ju, K. Lee, and D. B. Janes, Nano Lett. **5**, 2281 (2005).
[19]T. H. Moon, M. C. Jeong, B. Y. Oh, M. H. Ham, M. H. Jeun, W. Y. Lee, and J. M. Myoung, Nanotechnology **17**, 2116 (2006).
[20]T. J. Coutts, D. L. Young, and X. N. Li, MRS Bull. **25**, 58 (2000).
[21]R. Groenen, E. R. Kieft, J. L. Linden, and M. C. M. Van De Sanden, J. Electron. Mater. **35**, 711 (2006).
[22]P. Y. Emelie, J. D. Phillips, B. Buller, and U. D. Venkateswaran, J. Electron. Mater. **35**, 525 (2006).
[23]J. Kim, S. Jung, E. J. Choi, K. Kim, K. Lee, and S. Im, Appl. Phys. Lett. **93**, 241902 (2008).
[24]C. A. Wolden, T. M. Barnes, J. B. Baxter, and E. S. Aydil, J. Appl. Phys. **97**, 043522 (2005).
[25]L. E. Greene, B. D. Yuhas, M. Law, D. Zitoun, and P. D. Yang, Inorg. Chem. **45**, 7535 (2006).
[26]M. Von Allmen and A. Blatter, *Laser-Beam Interactions with Materials: Physical Principles and Applications*, 2nd ed. (Springer, Berlin, 1995), p. 194.
[27]O. Ambacher, W. Rieger, P. Ansmann, H. Angerer, T. D. Moustakas, and M. Stutzmann, Solid State Commun. **97**, 365 (1996).
[28]W. B. Jackson, N. M. Amer, A. C. Boccara, and D. Fournier, Appl. Opt. **20**, 1333 (1981).
[29]N. Kashii, H. Maekawa, and Y. Hinatsu, J. Am. Ceram. Soc. **82**, 1844 (1999).
[30]R. Hansson, P. C. Hayes, and E. Jak, Metall. Mater. Trans. B **35**, 633 (2004).
[31]T. Tsubota, M. Ohtaki, K. Eguchi, and H. Arai, J. Mater. Chem. **7**, 85 (1997).
[32]S. Yoshioka, F. Oba, R. Huang, I. Tanaka, T. Mizoguchi, and T. Yamamoto, J. Appl. Phys. **103**, 014309 (2008).
[33]T. Minami, H. Sato, K. Ohashi, T. Tomofuji, and S. Takata, J. Cryst. Growth **117**, 370 (1992).
[34]S. L. Dexheimer, *Terahertz Spectroscopy: Principles and Applications* (CRC Press, Boca Raton, FL, 2007).
[35]K. Ellmer, A. Klein, and B. Rech, in *Springer Series in Materials Science* (Springer-Verlag, Berlin, Heidelberg, 2008), Vol. 104.
[36]T. Pisarkiewicz, K. Zakrzewska, and E. Leja, Thin Solid Films **174**, 217 (1989).
[37]A. V. Singh, R. M. Mehra, A. Yoshida, and A. Wakahara, J. Appl. Phys. **95**, 3640 (2004).
[38]O. Wunnicke, Appl. Phys. Lett. **89**, 083102 (2006).
[39]C. Reese and Z. N. Bao, J. Appl. Phys. **105**, 024506 (2009).
[40]J. F. Stebbins, Chem. Mater. **19**, 1862 (2007).
[41]N. Roberts, R. P. Wang, A. W. Sleight, and W. W. Warren, Phys. Rev. B **57**, 5734 (1998).